A

DAPI/ɣ-tubulin(centrosome)

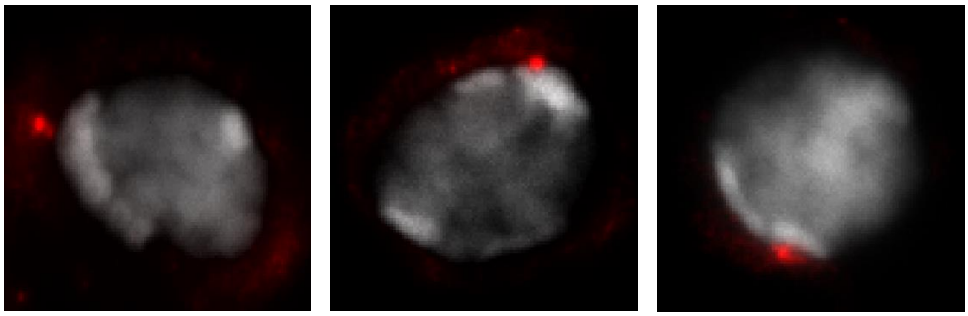

ɣ-tubulin/ heterochromatin patch(DAPI) (% cells, n=30)	Associated	No associated
	87	13

B

α-tubulin/ɣ-tubulin

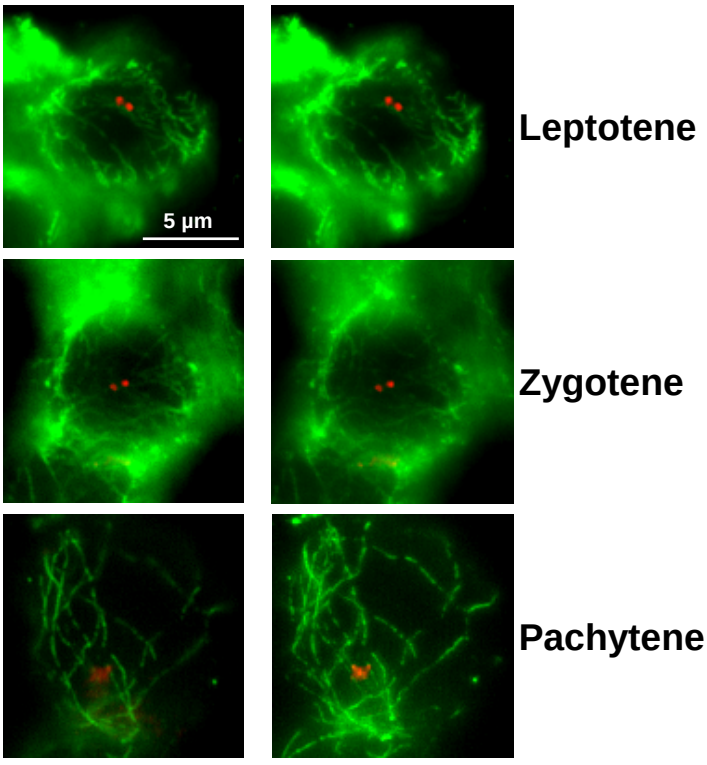

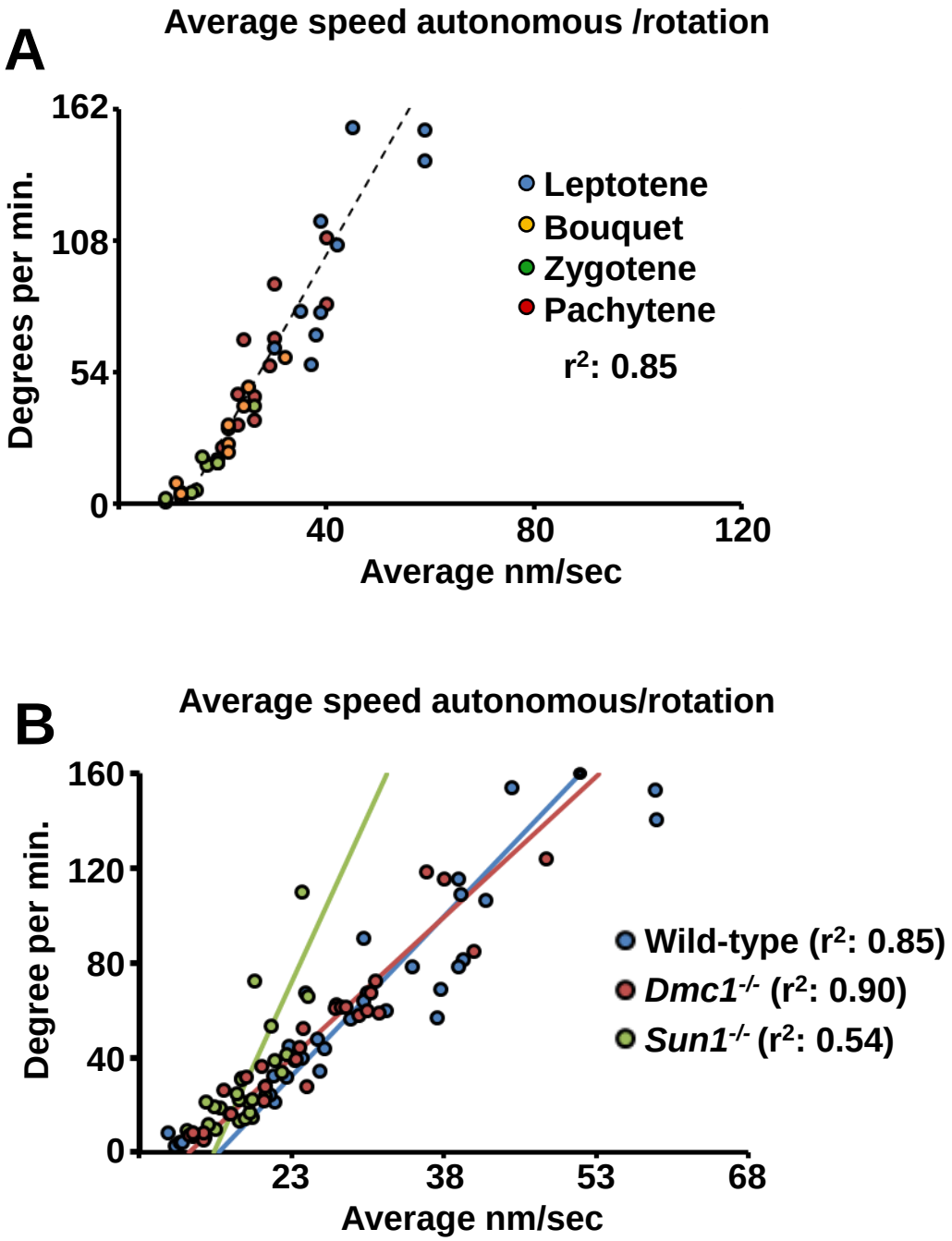
A
Average speed autonomous /rotation
Degrees per min.
162
108
54
0
40
80
120
Average nm/sec
Leptotene
Bouquet
Zygotene
Pachytene
r²: 0.85
B
Average speed autonomous/rotation
Degree per min.
160
120
80
40
0
23
38
53
68
Average nm/sec
Wild-type (r²: 0.85)
Dmc1-/- (r²: 0.90)
Sun1-/- (r²: 0.54)

Figure S3

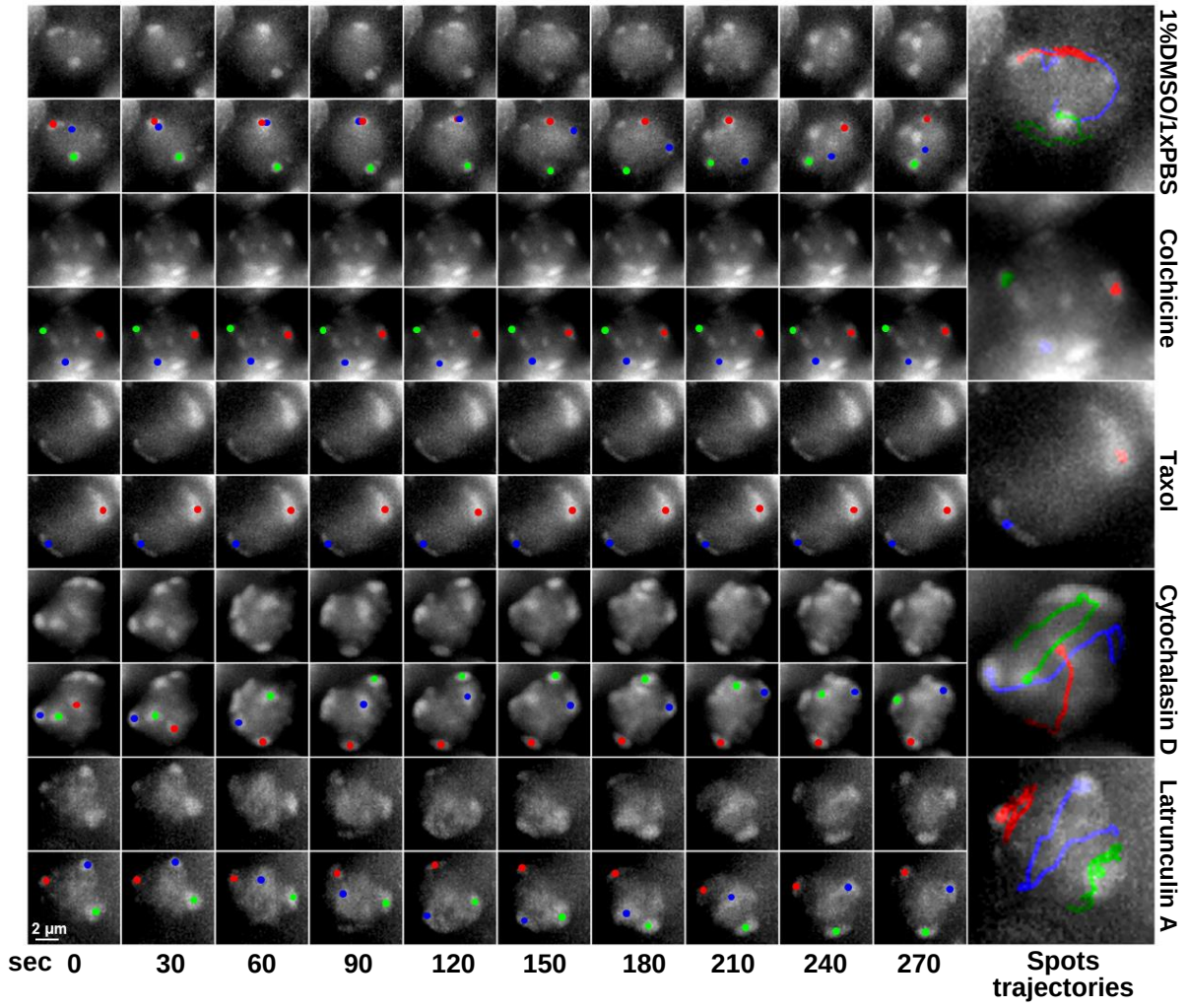
A
1%DMSO/1xPBS
Colchicine
Taxol
Cytochalasin D
Latrunculin A
2 µm
sec 0 30 60 90 120 150 180 210 240 270
Spots trajectories

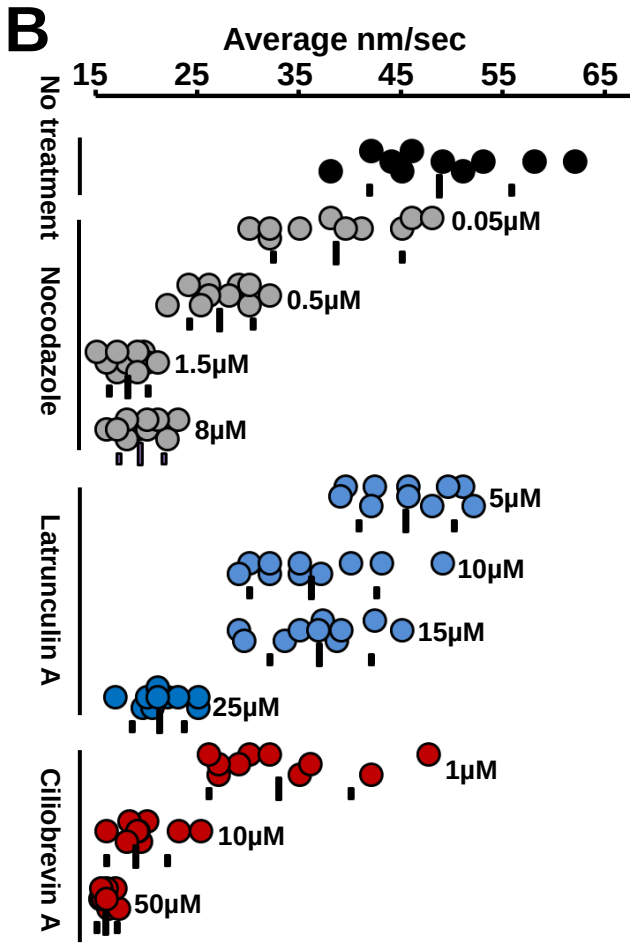
B
Average nm/sec
15 25 35 45 55 65
No treatment
Nocodazole
0.05µM
0.5µM
1.5µM
8µM
Latrunculin A
5µM
10µM
15µM
25µM
Ciliobrevin A
1µM
10µM
50µM

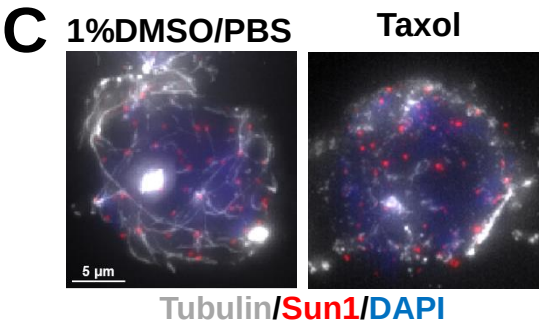
C
1%DMSO/PBS
Taxol
5 µm
Tubulin/Sun1/DAPI

Figure S4

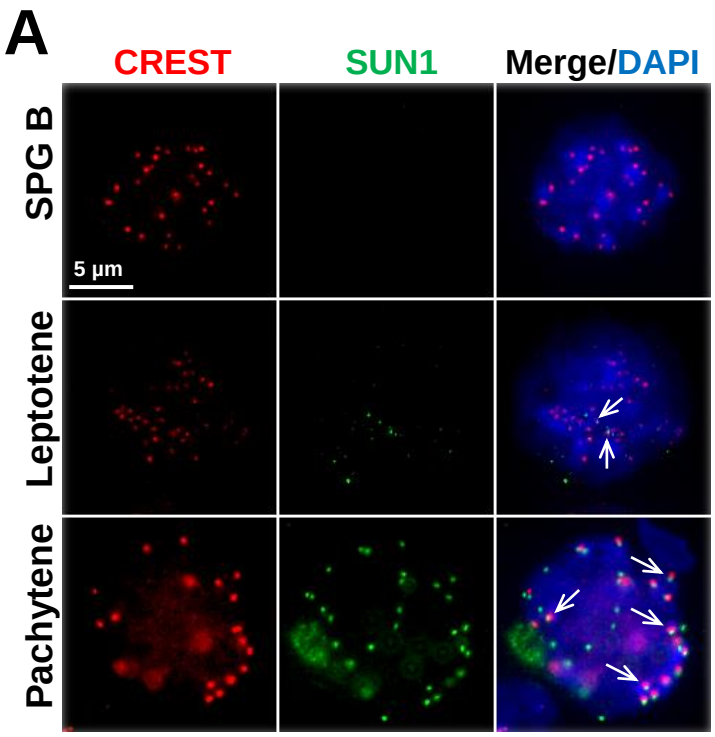
A
CREST
SUN1
Merge/DAPI
SPG B
Leptotene
Pachytene
5 µm

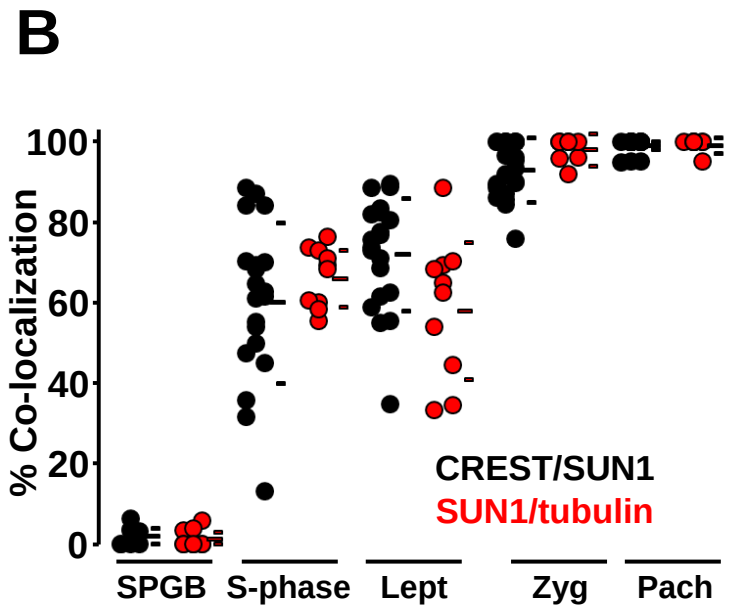
B
% Co-localization
100
80
60
40
20
0
CREST/SUN1
SUN1/tubulin
SPGB
S-phase
Lept
Zyg
Pach

SUPPLEMENTAL INFORMATION

SUPPLEMENTAL FIGURES AND LEGENDS

Figure S1 in relation to Figures 2 and 3. Relationships between the centrosome, telomere clustering and α-tubulin cable network in prophase spermatocytes. A. Example of bouquet nuclei showing clustered proximal telomeres (DAPI) close to the centrosome and quantitation of these nuclei. **B**. Representative images of the immunolocalization of α-tubulin and ɣ-tubulin in leptotene, zygotene, and pachytene spermatocytes. Single slices (left panel) and maximum intensity projections (MIP; right panel) are shown. Magnification bar represents 5µm.

Figure S2 in relation to Figure 3 and Figure 5. Characterization of chromosome movements in mouse spermatocytes. A. Average speed of autonomous movements versus degree of rotation for spot movements in prophase I nuclei. The regression line corresponds to all stages of prophase I. **B.** Plot of residual speed versus rotation for zygotene nuclei in wild-type, *Dmc1*$^{-/-}$, and *Sun1*$^{-/-}$ spermatocytes. The trend lines and linear regression values are shown.

Figure S3 in relation to Figure 4. Effect of microtubule, actin, and dynein inhibitors on the speed of RPMs. A. Maximum-intensity projections of time-lapse images of wild-type zygotene nuclei treated with microtubule and actin inhibitors. For each nucleus, the peri-centromeric heterochromatin spots (top panel) and trajectory of selected spots (represented in different colors; bottom panel) are shown. Magnification bar represents 2µm. **B.** Quantitation of RPMs in zygotene spermatocytes after microtubules incubation with 1% DMSO or microtubule (0.05-8µM), actin (5-25 µM) or dynein (1-50 µM) inhibitors; horizontal lines indicate the median and standard deviation values. **C.** Maximum-intensity projections of representative pachytene

spermatocytes immunostained for α-tubulin and SUN1 after the indicated treatments. Magnification bar represents 5μm.

Figure S4 in relation to Figure 6. Visualization of KASH5-SUN1 complexes coupling telomeres to cytoskeletal dynein-microtubule cables. A. Example of wild-type B type spermatogonia (SPG B), leptotene, and pachytene spermatocytes showing co-localization of CREST (marker of proximal telomeres) and SUN1. The scale bar represents 5 μm and applies to all images. Arrows indicate examples of sites of CREST/SUN1 co-localization. **B**. Quantitation of CREST-SUN1 and SUN1-αtubulin co-localization in B type spermatogonia, pre meiotic s-phase (S-phase), and prophase I spermatocytes.

SUPPLEMENTAL MOVIES

Supplemental Movie 1 in relation to Figure 2. RPMs in wild-type leptotene. Example of RPMs in wild-type leptotene spermatocytes.

Supplemental Movie 2 in relation to Figure 2. RPMs in wild-type zygotene. Example of RPMs in wild-type spermatocytes at zygotene stage.

Supplemental Movie 3 in relation to Figure 2. RPMs in wild-type bouquet. Example of RPMs in wild-type bouquet spermatocytes.

Supplemental Movie 4 in relation to Figure 2. RMPs in ild-type pachytene. Example of RPMs in wild-type pachytene spermatocytes.

Supplemental Movie 5 in relation to Figure 3. Nuclear rotation and independent chromosome movements. Depiction of procedure to determine autonomous and rotational chromosome movements in a wild-type spermatocyte.

Supplemental Movie 6 in relation to Figure 3. Simulation of chromosome movements. Simulation of chromosome movements in a wild-type spermatocyte describes the observed behaviors of the pericentromeric spots.

Supplemental Movie 7 in relation to Figure 5. Sun $1^{-/-}$ mutant. Example of RPMs in $Sun1^{-/-}$ spermatocytes. Note the significantly reduction in RPMs.

Supplemental Movie 8 in relation to Figure 5. Sun $1^{-/-}$ chromosome movements deconvolution. Determination of deficient autonomous and rotational chromosome movements in a $Sun1^{-/-}$ spermatocyte.

SUPPLEMENTAL EXPERIMENTAL PROCEDURES

Preparation and Imaging of Seminiferous Tubules

Seminiferous tubules of one month-old mice were transferred into Eppendorf tubes containing 1 ml Hoechst 33342 chromatin dye (0.005-0.02 mg/ml) in DMEM cell culture media lacking pH indicator (cat. #2015-11, Gibco). After 30 min incubation at 32°C, the tubules were rinsed and stored in DMEM at 32°C until analysis (not exceeding 3 h). Tubules were placed between a glass bottom dish (cat. #HBSt-5030, Willco Wells) and coverslip separated by glass beads in DMEM and sealed with VALAP. Four-dimensional movie stack images (16 slices with 1 μm steps) were acquired every 10 sec for the indicated times using a Zeiss Axioplan 2ie fitted with a 63X 1.4NA objective, Roper CoolSnap camera and custom acquisition software.

It is important to emphasize that Hoechst 33342 staining of heterochromatin spots is pericentromeric and in the mouse, represents half of the telomeres in the nucleus. During the ~10 days that spermatocytes spend in pachytene, they move away from the seminiferous tubule wall to a location deep inside the tubule where spherical aberrations prohibit clear imaging using wide-field, high numerical aperture optics. Thus, the meiotic prophase stages after pachytene were not analyzed in this work.

To reduce the effects of noise and anisotropic resolution (0.1 μm along the X and Y axes and 1.0 μm along the Z axis), spot positions were smoothed by taking the average of the positions in a moving window over every three time-points.

Small molecule Inhibitor Treatment of Seminiferous Tubule Explants

Seminiferous tubules treated with small molecule inhibitors were prepared for imaging as described under “Preparation and Imaging of Seminiferous Tubules”. Small molecule inhibitors (final concentration as indicated) were added to the Eppendorf tubes containing 1 ml Hoechst 33342 chromatin dye (0.005-0.02 mg/ml) in DMEM. After 30 min incubation at 32°C, the tubules were rinsed and stored in DMEM at 32°C until analysis.

Analysis and Quantification of Autonomous and Rotational Chromosome Movements

To determine the contribution of nuclear rotation to total RPM, we began by estimating the center of each nucleus and then calculating the axis/axes of rotation. We estimated the center of the nuclei by finding the best fitting sphere (in a least-squares sense) for the coordinates of the apparently peripheral spots for all time points for each nucleus. Next, we applied several methods to estimate the axes of rotation and assessed the accuracies of these methods by “decoding” synthetic datasets. Synthetic datasets were generated by: (1) randomly placing points on the surface of a sphere; (2) rotating the sphere around a fixed axis or varying the axes

by a given number of degrees per step; (3) adding movement along a defined vector for one spot alone (in addition to rotation); (4) mapping the point positions at each step onto a grid with the same spacing used to acquire the image stacks (0.1 micron/pixel in X and Y, 1.0 micron/pixel in Z); and (5) measuring rotation and speeds in the synthetic image datasets using the same software protocols to be applied to the experimental data. Two methods gave similar results. In the first, a single axis of rotation was calculated as an average for the entire time-course by averaging the cross products of the vectors defined by successive spot positions. Then, for each spot, the angle of rotation around this axis was calculated for each step (*i.e*., from time-point tn to tn+1) and the nucleus was "unspun" by the median of the angles for that step. In the second method, the axis of rotation was calculated separately for each step, omitting the data for any spots within 26^{o} of the pole (where small amounts of noise in the measurements outsized the impacts on the outcome). Then, for each (non-omitted) spot, the angle of rotation around the axis defined for that step was calculated, and the nucleus was unspun by the average angle for that step. In both methods, nuclei were unspun by two passes through the data. It is important to note that the relative positions of the spots at each time-point remain unchanged using either approach. Once unspun, movements were measured again, as "residual" movements that were a combination of the true autonomous movements plus any noise from miscalculated rotation. The first approach proved less susceptible to inaccurate positioning or small numbers of spots, but underestimated total spin and overestimated autonomous movements. The second approach captured more of the "wobble" of nuclear rotation and minimized autonomous movements, while potentially overestimating the degrees of rotation. Detailed examination of spot movements suggested that nucleus "wobble" indicated the mechanism underlying the movements, so only measurements made using the second approach are reported here.

Spermatocyte Squash Preparation

Testes from adult male C57BL/6 mice 4–8 weeks old were removed, detunicated, and seminiferous tubules processed for squashing as previously described (Parra et al., 2009). Briefly, seminiferous tubules were fixed in freshly prepared 2% formaldehyde in 1× PBS containing 0.1% Triton X-100. After 5 min, several seminiferous tubule fragments were placed on a slide and squashed, and the coverslip removed after freezing in liquid nitrogen. Samples were washed with 1× PBS and stored up to 4 days before use.

Antibodies

The following antibodies were used: Rabbit anti-SYCP1 (Novus), 1:300; chicken anti-SYCP3 antibody raised against full length SYCP3, 1:300; human anti-CREST (Antibody incorporated), 1:50; mouse anti-α-Tubulin (Sigma), 1:100; mouse anti-γ-Tubulin (Sigma), 1:100; rabbit anti-SUN1 (Sigma), 1:50; rabbit anti-dynein (Covance), 1:100; and rabbit anti-Kash5 (Horn et al., 2013), 1:100.

Immunostaining of Fixed Spermatocytes

Incubations with primary antibodies were carried out for 12 h at 4°C in 1× PBS plus BSA 2%. Following three washes in 1× PBS, slides were incubated for 1 h at room temperature with secondary antibodies. A combination of fluorescein isothiocyanate (FITC)-conjugated goat anti-rabbit IgG (Jackson laboratories) with Rhodamine-conjugated goat anti-mouse IgG and Cy5-conjugated goat anti-human IgG each diluted 1:300 were used for simultaneous triple immunolabeling. Slides were subsequently counterstained for 3 min with 2 µg/ml DAPI containing Vectashield mounting solution (Vector Laboratories) and sealed with nail varnish.

SUPPLEMENTAL REFERENCES

Parra, M.T., Gomez, R., Viera, A., Llano, E., Pendas, A.M., Rufas, J.S., and Suja, J.A. (2009). Sequential assembly of centromeric proteins in male mouse meiosis. PLoS Genet *5*, e1000417.